

3-Hz Subthreshold Oscillations of CA2 Neurons *In Vivo*Nobuyoshi Matsumoto,¹ Kazuki Okamoto,¹ Yuki Takagi,¹ and Yuji Ikegaya^{1,2*}

ABSTRACT: The CA2 region is unique in the hippocampus; it receives direct synaptic innervations from several hypothalamic nuclei and expresses various receptors of neuromodulators, including adenosine, vasopressin, and oxytocin. Furthermore, the CA2 region may have distinct brain functions, such as the control of instinctive and social behaviors; however, little is known about the dynamics of the subthreshold membrane potentials of CA2 neurons *in vivo*. We conducted whole-cell current-clamp recordings from CA2 pyramidal cells in urethane-anesthetized mice and monitored the intrinsic fluctuations in their membrane potentials. The CA2 pyramidal cells emitted spontaneous action potentials at mean firing rates of ~0.8 Hz. In approximately half of the neurons, the subthreshold membrane potential oscillated at ~3 Hz. In two neurons, we obtained simultaneous recordings of local field potentials from the CA1 *stratum radiatum* and demonstrated that the 3-Hz oscillations of CA2 neurons were not correlated with CA1 field potentials. In tetrodotoxin-perfused acute hippocampal slices, the membrane potentials of CA2 pyramidal cells were not preferentially entrained to 3-Hz sinusoidal current inputs, which suggest that intracellular 3-Hz oscillations reflect the neuronal dynamics of the surrounding networks. © 2016 Wiley Periodicals, Inc.

KEY WORDS: CA2; 3 Hz; *in vivo* whole-cell recording; membrane potential; oscillation

Instead, CA2 neurons have been demonstrated to be unique in several ways: (i) they receive direct axonal afferents from several hypothalamic nuclei, such as the supramammillary nucleus, the tuberomammillary nucleus, and the paraventricular nucleus (Amaral and Lavanex, 2007), (ii) they exhibit high expression of neuromodulator receptors, such as vasopressin 1b receptors, oxytocin receptors, and adenosine A1 receptors (Amaral and Lavanex, 2007), and (iii) the CA2 region is involved in aggressive behaviors (Pagani et al., 2015) and social learning (Hitti and Siegelbaum, 2014; Piskorowski et al., 2016; Smith et al., 2016). Consistent with these observations, the firing properties of CA2 place cells have been reported to differ from CA1 and CA3 place cells (Mankin et al., 2015; Kay et al., 2016). Nevertheless, electrophysiological evidence that bridges anatomical, histological, and behavioral findings remains scant. In this study, we investigated the dynamics of the membrane potentials (V_m) of CA2 neurons using *in vivo* whole-cell recordings from urethane-anesthetized mice.

INTRODUCTION

The pyramidal field of the hippocampus is divided into three subareas, including the CA1, CA2, and CA3 regions. However, compared with the CA1 or CA3 regions, the CA2 region has not been extensively investigated, probably because the CA2 region is anatomically small and is not part of the classical tri-synaptic pathway that extends from the dentate gyrus to the CA1 region (Andersen et al., 1971). Recent evidence has indicated that the properties and functions of CA2 neurons cannot be estimated from the current knowledge regarding CA1 and CA3 neurons (Jones and McHugh, 2011; Caruana et al., 2012; Kay et al., 2016).

MATERIALS AND METHODS

Animal Ethics

Animal experiments were performed with the approval of the animal experiment ethics committee at the University of Tokyo (approval numbers: 24-8 and 26-5) and in accordance with the University of Tokyo guidelines for the care and use of laboratory animals. These experimental protocols were conducted in accordance with the Fundamental Guidelines for the Proper Conduct of Animal Experiments and Related Activities in Academic Research Institutions (Ministry of Education, Culture, Sports, Science and Technology, Notice No. 71 of 2006), the Standards for Breeding and Housing of and Pain Alleviation for Experimental Animals (Ministry of the Environment, Notice No. 88 of 2006) and the Guidelines on the Method of Animal Disposal (Prime Minister's Office, Notice No. 40 of 1995).

Surgery

Whole-cell recordings were obtained from postnatal 21- to 35-day-old male ICR mice (Japan SLC, Shizuoka, Japan) as previously described (Ishikawa et al.,

¹Laboratory of Chemical Pharmacology, Graduate School of Pharmaceutical Sciences, The University of Tokyo, Bunkyo-ku, Tokyo, Japan; ²Center for Information and Neural Networks, National Institute of Information and Communications Technology, Suita City, Osaka, Japan

Grant sponsor: Grants-in-Aid for Science Research A; Grant number: 26250003; Grant sponsor: Grants-in-Aid for Science Research on Innovative Areas "Mental Time"; Grant number: 25119004.

*Correspondence to: Yuji Ikegaya, PhD, Laboratory of Chemical Pharmacology, Graduate School of Pharmaceutical Sciences, The University of Tokyo, 7-3-1 Hongo, Bunkyo-ku, Tokyo 113-0033, Japan.

E-mail: yuji@ikegaya.jp

Accepted for publication 6 September 2016.

DOI 10.1002/hipo.22657

Published online 20 September 2016 in Wiley Online Library (wileyonlinelibrary.com).

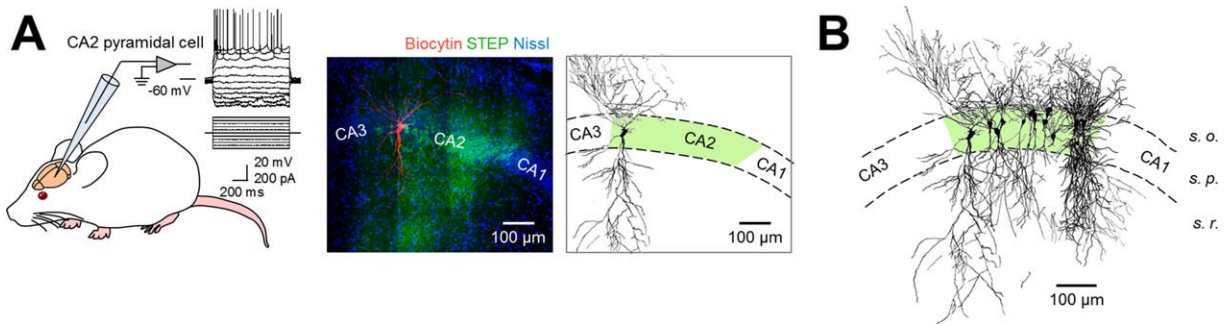


FIGURE 1. *In vivo* patch-clamp recordings from CA2 pyramidal cells. *A, Left:* A CA2 pyramidal neuron was current-clamp recorded in a urethane-anesthetized mouse, and biocytin was injected through a whole-cell pipette. *Middle:* The recorded neuron was reconstructed *post hoc* using a confocal microscope (red).

The section was stained with anti-STEP (green, a CA2 neuron marker) and NeuroTrace (blue). *Right:* The neuronal morphology was digitally traced in the *right inset*. *B,* All 16 CA2 pyramidal cells recorded are superimposed onto the *stratum pyramidale* diagram. [Color figure can be viewed at wileyonlinelibrary.com.]

2014; Funayama et al., 2015). The mice were anesthetized with urethane (2.25 g kg^{-1} , intraperitoneal [i.p.]), and 1.0% lidocaine was subcutaneously applied to the surgical region. Anesthesia was confirmed by the lack of paw withdrawal, whisker movement, and eye blink reflexes. The skin was subsequently removed from the head, and the animal was implanted with a metal head-holding plate. A craniotomy ($2.5 \times 2.0 \text{ mm}^2$) was performed, which was centered at 2.0 mm posterior to the bregma and 2.5 mm ventrolateral to the sagittal suture, and the neocortex above the hippocampus was aspirated (Kuga et al., 2011; Sakaguchi et al., 2012). The exposed hippocampal window was covered with 1.7% agar at a thickness of 1.5 mm. Throughout the experiments, a heating pad maintained the rectal temperature at 37°C . For extracellular recordings, an additional craniotomy ($2.5 \times 0.5 \text{ mm}^2$) was performed, which was centered at 1.7 mm posterior to the bregma and 0.4 mm ventrolateral to the sagittal suture. For the experiments that used awake mice, the mice were anaesthetized with ketamine (50 mg kg^{-1} , i.p.) and xylazine (10 mg kg^{-1} , i.p.) and were subsequently implanted with metal head-holding plates. After 2 days of recovery, the mice received head-fixation training on a custom-made stereotaxic fixture for $1\text{--}3 \text{ h day}^{-1}$. Training was terminated when the mice learned to remain quiet (Abe et al., 2014).

In Vivo Electrophysiology

Current-clamped recordings were obtained from hippocampal CA1 and CA2 neurons at depths of $100\text{--}550 \mu\text{m}$ from the dorsal alveus using borosilicate glass pipettes ($3.5\text{--}6.5 \text{ M}\Omega$). The intra-pipette solution consisted of the following reagents: 135 mM K-gluconate, 4 mM KCl, 10 mM HEPES, 10 mM Na_2 -phosphocreatine, 4 mM Mg-ATP, 0.3 mM Na_2 -GTP, 0.3 mM EGTA, and 0.2% biocytin. The solution was adjusted to pH 7.3 and $285\text{--}290 \text{ mOsm kg}^{-1}$. The signal was amplified with a MultiClamp 700B, analyzed with pCLAMP10.1 (Molecular Devices, Union City, CA) and digitized at 20 kHz. At the beginning of each experiment, 500-ms rectangular

currents of $200\text{--}200 \text{ pA}$ were injected into the cells at steps of 20 pA, and the spike responses were examined. Regular-spiking neurons were selected for analysis (Fig. 1A left). The liquid junction potential was nulled offline. Cells were discarded when the series resistance exceeded $75 \text{ M}\Omega$ or the mean liquid junction-corrected resting potential exceeded -64 mV . Moreover, recordings were truncated when the spike peak decreased below -20 mV or the resting potential increased by more than 8 mV from its value at the onset of the recording. Local field potentials (LFPs) were obtained from the CA1 *stratum radiatum* at depths of $1100\text{--}1500 \mu\text{m}$ from the brain surface using borosilicate glass electrodes ($1\text{--}3 \text{ M}\Omega$) filled with artificial cerebrospinal fluid (aCSF), which was composed of 127 mM NaCl, 1.6 mM KCl, 1.24 mM KH_2PO_4 , 1.3 mM MgSO_4 , 2.4 mM CaCl_2 , 26 mM NaHCO_3 , and 10 mM glucose. The recording sites for CA1 LFPs were at least $500 \mu\text{m}$ apart from that for CA2 V_m . Traces were band-pass filtered between 1 and 400 Hz. Data were analyzed offline using custom-written MATLAB routines.

In Vitro Electrophysiology

Postnatal 21- to 35-day-old male ICR mice were deeply anesthetized with isoflurane and decapitated. The brains were rapidly removed and horizontally sliced at a thickness of $400 \mu\text{m}$ using a vibratome in an ice-cold, oxygenated (95% O_2 , 5% CO_2) cutting solution, which was composed of 222.1 mM sucrose, 27 mM NaHCO_3 , 1.4 mM NaH_2PO_4 , 2.5 mM KCl, 1 mM CaCl_2 , 7 mM MgSO_4 , and 0.5 mM ascorbic acid (Mizunuma et al., 2014). After 30–45 min of recovery at 35°C , a slice was placed in a submerged chamber and was perfused at 2 mL min^{-1} with oxygenated aCSF at 35°C . CA1 and CA2 neurons were visually identified under infrared differential interference contrast microscopy and were current-clamped using borosilicate glass pipettes ($3\text{--}6 \text{ M}\Omega$) with the same intra-pipette solution used in the *in vivo* recordings. At the beginning of each experiment, 500-ms rectangular currents of $100\text{--}240 \text{ pA}$ were injected into the cells at steps of 20 pA, and

the spike responses were examined. Regular-spiking neurons were selected and were bath-perfused with 1 μM tetrodotoxin. In a single session, brief sinusoidal currents at 1–40 Hz and 3–5 s were injected into the neuron every 30 s (Zemankovics et al., 2010). This session was repeated 5 times. The series resistance of the recorded cell was determined at the beginning and end of each experiment. Data were rejected when the series resistance exceeded 35 M Ω or increased by 5%.

Histology

Following each experiment, the electrode was carefully withdrawn. The mice were transcardially perfused with 4% paraformaldehyde followed by overnight post-fixation. The brains were sagittally sectioned at a thickness of 100 μm using a vibratome. Acute slices were fixed overnight in 4% paraformaldehyde. The sections were incubated with 2 $\mu\text{g mL}^{-1}$ streptavidin-Alexa Fluor 594 conjugate and 0.2% Triton X-100 for 6 h, followed by incubation with 0.4% NeuroTrace 435/455 Blue Fluorescent Nissl Stain (Thermo Fisher Scientific; N21479) overnight. The tissue sections were subsequently incubated with the mouse primary antibody to STEP (Cell Signaling Technology; 4396S; 1:500) for 16 h at 4°C, followed by incubation with the secondary goat antibody to mouse IgG (Thermo Fisher Scientific; A-11001; 1:500) for 6 h at 4°C. Fluorescent images were acquired using a CV1000 confocal microscope (Yokogawa) and were subsequently merged.

Data Analysis

Data analyses were performed using MATLAB (MathWorks, Natick, MA), and the summarized data were reported as the means \pm standard deviations (SDs) unless otherwise specified. $P < 0.05$ was considered statistically significant.

To determine whether a neuron oscillated intracellularly at 3 Hz, we computed the auto-correlation function of its V_m across the whole recording time period and compared the oscillatory peak amplitude with its chance level. To estimate the chance level, we divided the original V_m traces into 100-ms segments, combined them in a randomly shuffled order, and generated a surrogate. We repeated this randomization and obtained 1,000 surrogates from each original trace. If the peak in the autocorrelation of the original trace between 0.25 and 0.5 s (that is, 2–4 Hz, respectively) was beyond the mean $\pm 6 \times \text{SD}$ in the autocorrelations of the surrogates, we defined the cell as an oscillating neuron.

To assess the spatial clustering of 3-Hz oscillating neurons, we linearly normalized the locations of individual cells within the CA2 *stratum pyramidale* as an ideal square space to ensure their coordinates ranged from 0 to 1. All datasets were subsequently pooled, and the geometric energy was calculated as follows (Makino et al., 2016):

$$\text{Energy} = \sum \frac{Z_i Z_j}{r_{ij}}, \quad (i \neq j),$$

where Z_i is 1 or 0 depending on whether or not, respectively, neuron i exhibits 3-Hz oscillations, and r_{ij} is the Euclidean distance between neurons i and j in the normalized coordinate. The geometric energy was compared with the chance level, which was estimated by surrogates in which the Z values were exchanged across all analyzed CA2 pyramidal cells. For surrogates, all 1,716 possible exchanges in the Z vector were generated. To estimate the asymmetry of the distribution of oscillating cells, we calculated the skewness for the horizontal or vertical axis as follows:

$$\text{Skewness} = \frac{\sum (x_i - m)^3}{N s^3},$$

where x_i is the normalized coordinate of an oscillating neuron i , and m and s represent the mean value and the SD, respectively, of the normalized coordinates of all oscillating neurons. N comprises the total number of 3-Hz oscillating neurons (here, $N = 7$). The skewness was compared with the chance level, which was estimated using the 1,716 surrogates.

To identify individual oscillating events, we used the wavelet transform. Any given time period was defined as a “3-Hz oscillation” period if the mean absolute value of its wavelet coefficient between 2–4 Hz exceeded the mean $\pm 2 \times \text{SD}$ of the values between 1–100 Hz. Likewise, a time period was defined as a “gamma oscillation” period if the absolute value of its wavelet coefficient between 30–90 Hz exceeded the mean $\pm 2 \times \text{SD}$ of the values between 1 and 100 Hz. To detect extracellular ripple oscillations, LFP traces were band-pass filtered at 150–250 Hz. Ripples were detected at a threshold at $6 \times \text{SD}$ of the baseline noise (Mizunuma et al., 2014). The detected events were subsequently scrutinized by eye and manually rejected if they were erroneously detected.

To determine the oscillation phase of an action potential that occurred at time t , we band-pass filtered the V_m traces of 3-Hz-oscillating CA2 neurons between 2 and 4 Hz and identified the times of the oscillatory cycle peaks immediately before and after the focused spikes (t_1 and t_2 , respectively) in the filtered trace. The spike phases were determined as $360 \times (t - t_1)/(t_2 - t_1)$ (Harvey et al., 2009). To calculate the mean angle θ among a set of $\theta_1, \theta_2, \dots, \theta_m$, we first regarded each angle as a vector of one unit length in the direction of the angle and composed a single resultant vector \vec{a} from all the vectors. Then, we calculated the mean resultant vector (that is, $\frac{1}{n} \vec{a}$), and defined the direction to which the mean resultant vector pointed as the mean angle θ . The circular standard deviation σ was defined as follows:

$$\sigma = \sqrt{-2 \ln L},$$

where L is the length of the mean resultant vector. Note that L varies between 0 and 1.

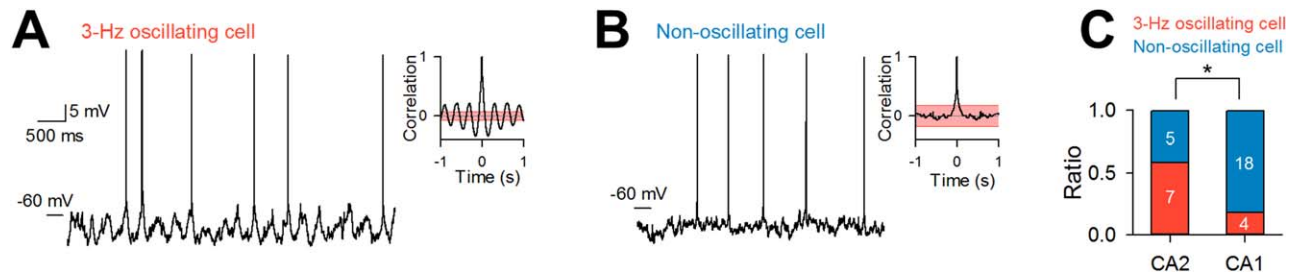


FIGURE 2. Half of the CA2 pyramidal cells exhibit intracellular 3-Hz oscillations. **A**, A representative V_m trace indicates a 3-Hz oscillating CA2 pyramidal cell and the autocorrelogram of its entire voltage trace with the 95% confidence interval (red). **B**, The image shows the same type of trace as in **A**, but it represents a

non-oscillating CA2 pyramidal neuron. **C**, Ratios are indicated for 3-Hz oscillating and non-oscillating pyramidal cells in the CA2 and CA1 regions. The numbers on the graphs represent the cell numbers. $*P = 0.026$, Fisher's exact test. [Color figure can be viewed at wileyonlinelibrary.com.]

RESULTS

Using the blind patch-clamp technique, we stereotaxically targeted the CA2 region in the dorsal hippocampus of the urethane-anesthetized mice (Fig. 1A left). Of the 63 mice attempted, we obtained whole-cell recordings from 54 neurons in 44 mice. After each experiment, we confirmed the location and morphology of the recorded neuron using biocytin reconstruction, immunostaining with an antibody against STEP, a CA2 marker, and counterstaining with NeuroTrace (Fig. 1A). Of the 54 recorded neurons, we succeeded in histological reconstruction of 53 (98.1%) neurons, which contained 15 CA2 pyramidal cells (Fig. 1B), 2 CA2 interneurons, 28 CA1 pyramidal cells, 3 CA1 interneurons, and 5 unidentified cells. To ensure the reliability of the electrophysiological measurements, we analyzed only 12 CA2 and 22 CA1 neurons that passed our rejection criteria. Under “ $I = 0$ ” conditions, the mean resting $V_{m,s}$ of the CA2 and CA1 neurons were -66.1 ± 0.8 and -68.1 ± 1.1 mV, respectively (mean \pm standard error of the mean [SEM] of 12 and 22 cells, respectively, $P = 0.23$, $t_{32} = 1.23$, Student's t test). The rates of spontaneous action potentials were 0.81 ± 0.35 Hz in CA2 and 1.07 ± 0.43 Hz in CA1 ($P = 0.69$, $t_{32} = 0.40$). The cell resistances (R_m) were 71.7 ± 16.8 M Ω in CA2 and 77.8 ± 9.8 M Ω in CA1 ($P = 0.75$, $t_{32} = 0.32$). None of these parameters were significantly different between the CA2 and CA1 neurons.

During these experiments, we determined that a subgroup of the CA2 pyramidal cells often exhibited periodic oscillations in the subthreshold V_m (Fig. 2A). To identify the characteristics of the oscillations in individual cells, we computed the autocorrelation functions of V_m across all recording periods. Some neurons exhibited fluctuated autocorrelations at time-intervals of 0.25–0.5 s, which indicates sub-theta V_m oscillations (Fig. 2A inset), whereas other neurons exhibited no apparent oscillations (Fig. 2B). To statistically assess the oscillations, we compared the oscillatory peaks to the chance level. If the peak of the original autocorrelation between 0.25 and 0.5 s was beyond the chance level, we classified the cell as an oscillating neuron

(Fig. 2A,B insets). This classification indicated that 7 of the 12 CA2 cells (58.3%) exhibited subthreshold V_m oscillations, whereas only 4 of the 22 CA1 pyramidal cells (18.2%) exhibited V_m oscillations (Fig. 2C). The ratio of oscillating cells was significantly higher in the CA2 region compared with the CA1 region (odds ratio = 6.30, $P = 0.026$, Fisher's exact test). The mean oscillation frequencies in the CA2 and the CA1 were 3.1 ± 0.7 Hz and 3.1 ± 0.2 Hz, respectively, and did not differ between them (mean \pm SD of 7 CA2 cells and 4 CA1 cells, respectively; $P = 0.96$, $t_9 = 0.05$, Student's t -test). Thus, the oscillations are referred to herein as “3-Hz” oscillations.

Oscillating and non-oscillating CA2 cells did not differ in the resting potential (-67.4 ± 3.0 mV in the oscillating cells versus -64.3 ± 0.8 mV in the non-oscillating cells; $P = 0.069$, $t_{10} = 2.04$, Student's t -test), cell resistance (69.0 ± 57.9 versus 75.5 ± 58.8 M Ω , respectively; $P = 0.87$, $t_{10} = 0.17$), or spontaneous firing rate (1.17 ± 1.44 versus 0.30 ± 0.38 Hz, respectively; $P = 0.25$, $t_{10} = 1.20$). The oscillating cells appeared to be evenly distributed in the CA2 *stratum pyramidale* (Fig. 3A). To quantify the distribution patterns, we analyzed the spatial clustering and spatial asymmetry of the locations of the oscillating cells. We measured spatial clustering using the geometric energy (Makino et al., 2016). The geometric energy was not significantly higher than the chance distribution, which was estimated in all possible 1,716 cell-shuffled surrogates (Fig. 3B, $P = 0.38$). To measure the spatial asymmetry of the oscillating cell locations in the CA2 *stratum pyramidale*, we used Pearson's moment coefficients of skewness along the CA3-to-CA1 transverse axis (Fig. 3C, horizontal) and the superficial-to-deep axis (Fig. 3D, vertical). The Pearson's moment coefficients of the real data were not significantly larger than those of the 1,716 cell-shuffled surrogates ($P = 0.39$ and 0.37 , respectively). In the CA1 region, 2 of 4 oscillating cells were located in the superficial layer of the CA1 *stratum pyramidale*, whereas the others were located in the deep layer. Thus, the oscillating cells did not exhibit a spatially biased distribution in either the CA2 or CA1 *stratum pyramidale*.

We subsequently investigated the temporal features of the 3-Hz V_m oscillations using the wavelet transform (Fig. 4A). In the spectrum, a power peak was evident at approximately 3

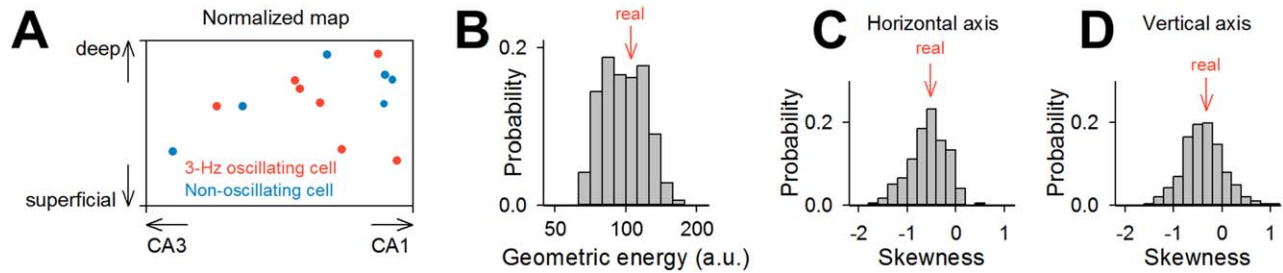


FIGURE 3. No spatial bias of 3-Hz oscillating CA2 pyramidal cells. *A*, The spatial locations of the cell bodies of 3-Hz oscillating (red) and non-oscillating cells (blue) are plotted in the normalized CA2 stratum pyramidale map. *B*, The geometric energy, which represents a measurement of spatial clustering of 3-Hz oscillating CA2 neurons (real), is compared with randomly chosen surrogates and indicates that 3-Hz oscillating neurons are not spatially

clustered in the CA2 stratum pyramidale. *C, D*, The skewnesses of the locations of 3-Hz oscillating neurons along the CA3-to-CA1 transverse axis (*C*, horizontal) and the superficial-to-deep axis (*D*, vertical) are compared with randomly chosen surrogates and indicate that the spatial distribution of 3-Hz oscillating neurons are not biased in the CA2 stratum pyramidale. [Color figure can be viewed at wileyonlinelibrary.com.]

Hz; however, it was not continuous during the entire recording period, which suggests that 3-Hz oscillations are temporally fragmented and occur as intermittent events. Thus, we statistically defined “3-Hz oscillation” periods by comparing its oscillation power to the chance level and defined a single continuous period as an oscillation event. The oscillation events occurred 8.8 ± 3.3 times per minute (Fig. 4B,

mean \pm SD of 7 oscillating cells), and a single event persisted for 5.9 ± 11.5 s (Fig. 4B, mean \pm SD of 127 events). The firing rates during the oscillation period were 1.21 ± 1.44 Hz (mean \pm SD of 7 oscillating cells) and were not significantly different from the rates of the non-oscillation period, 1.20 ± 1.43 Hz (mean \pm SD of 7 oscillating cells) ($P = 0.97$, $t_6 = 0.04$, paired t -test). The mean phase of individual action

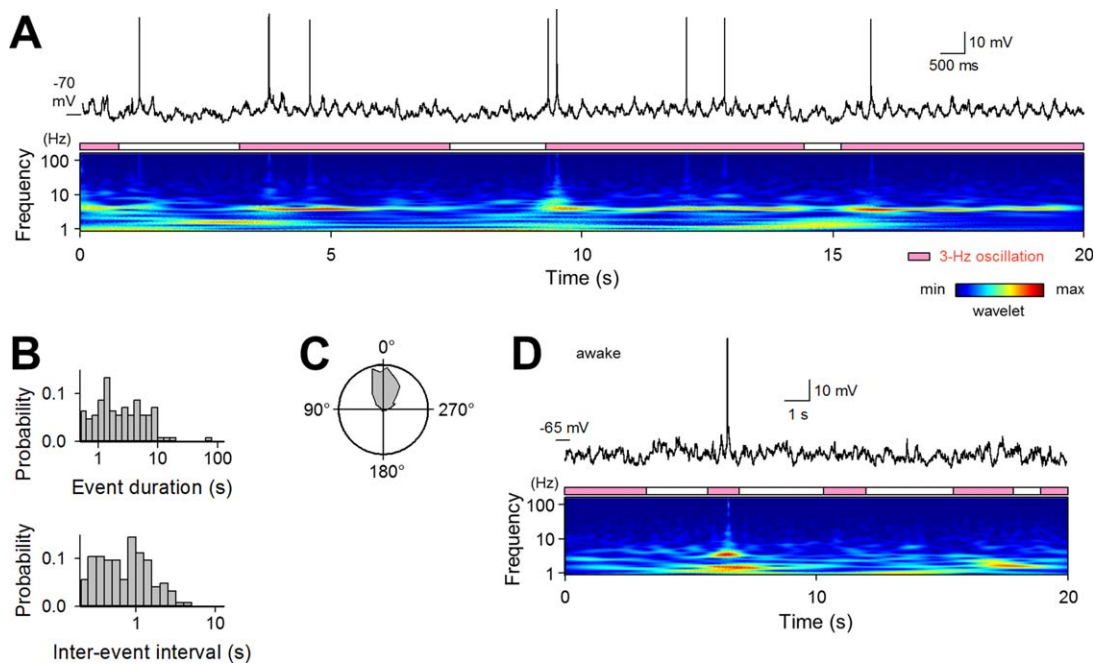


FIGURE 4. CA2 3-Hz oscillations are intermittent. *A*, A representative V_m trace of a CA2 pyramidal cell in a urethane-anesthetized mouse (top) and its wavelet spectrum (bottom) are shown. The periods in which the powers of the 3-Hz oscillations were significantly increased compared with the 1–100-Hz oscillations are indicated in pink. *B*, Distributions of the durations of individual 3-Hz oscillation events (left) and the time-intervals between the neighboring 3-Hz oscillation events (right) are

represented. $n = 127$ events from 7 oscillating cells. *C*, Probability density distribution of 3-Hz cycle phases at which action potentials occurred during 3-Hz oscillation events. $n = 1,090$ spikes in 7 cells. *D*, The image shows the same type of trace and spectrum as in *A*, but it represents a CA2 pyramidal cell recorded in an awake, head-restricted mouse. [Color figure can be viewed at wileyonlinelibrary.com.]

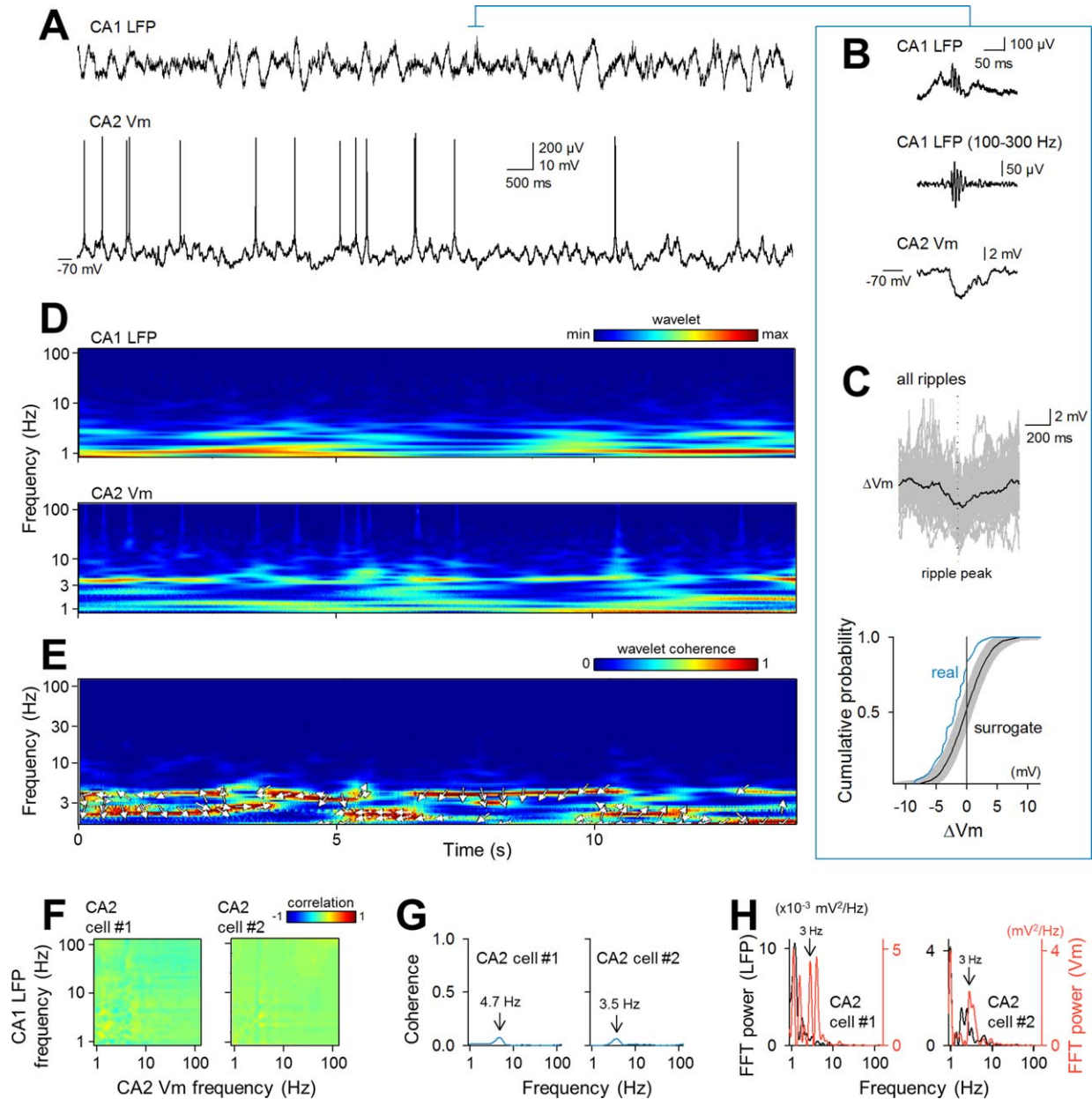


FIGURE 5. CA2 3-Hz oscillations do not correlate with CA1 LFPs. *A*, Simultaneous recordings of CA1 LFPs (*top*) and the V_m of a CA2 pyramidal cell (*bottom*) are represented. *B*, A representative CA1 LFP and CA2 V_m during a CA1 SW-R event indicates that the CA2 pyramidal cell exhibited a transient hyperpolarization during the SW-R. *C*, The mean CA2 V_m (*black*) during a total of 43 CA1 SW-R events were superimposed onto all individual V_m traces (*gray*) (*top*). The *bottom* plot demonstrates a cumulative distribution of the V_m changes during 43 SW-R events recorded from 2 cells (*blue*) and its chance distribution estimated in randomly sampled V_m (black) with the 95% confidence interval (gray). The plot indicates that overall, CA2 pyramidal cells are hyperpolarized during SW-Rs. *D*, The wavelets are displayed for the two traces shown in *A*. *E*, The wavelet coherences between the two traces shown in *A* are displayed. In areas where the coherence exceeded 0.5, their phases, which indicate the relative coherent lag

between the CA1 LFP and the CA2 V_m , were calculated using the wavelet cross-spectra. The relative lags between the coherent signals were indicated by the *white* arrows so that rightward and upward arrows indicate 0° and 90° , respectively. Although the coherence was occasionally high (hot colors), the direction of the arrows (phase) drifted over time, indicating that the coherence was not stable and might appear by chance. Thus, we conclude that the CA1 LFP and the CA2 V_m were not coherent. *F*, Power correlations of the CA1 LFPs and CA2 V_m of two CA2 pyramidal cells are shown. *G*, The coherences between the CA1 LFPs and CA2 V_m in two CA2 pyramidal cells are indicated. *H*, The fast Fourier transform (FFT) spectra for the CA1 LFPs and the CA2 V_m in the two CA2 pyramidal neurons. The peaks are not overlapped around 3 Hz in either case. The analyses of *D* to *H* indicate that CA2 3-Hz oscillations are not correlated with CA1 LFPs. [Color figure can be viewed at wileyonlinelibrary.com.]

potentials during the oscillation events were $352^\circ \pm 45^\circ$ (Fig. 4C), indicating that the action potentials were significantly clustered around the peak (0°) of the intracellular 3-Hz oscillations ($P < 0.0001$, $V_{1,090} = 34.1$, V -test versus 0°).

We sought to repeat the same experiments using awake, head-restricted mice. Of 27 mice attempted, we succeeded in whole-cell recordings from one CA2 pyramidal cell. In this anecdotal recording, the CA2 neuron intermittently exhibited 3-Hz oscillations (Fig. 4D); however, the 3-Hz events were unlikely to exhibit the same pattern of stability during wakefulness as demonstrated in the anaesthetized animals.

In two anesthetized mice, we recorded LFPs from the CA1 region simultaneously with whole-cell patching from CA2 neurons (Fig. 5A). Similar to a recent report by other groups (Valero et al., 2015), we demonstrated that CA2 pyramidal cells exhibited an average pattern of transient hyperpolarizations during CA1 sharp wave-ripple events (Figs. 5B,C, $n = 43$ events from two cells). For individual sharp wave-ripple events, the neurons were hyperpolarized in $88.2\% \pm 11.8\%$ of the sharp wave-ripple events (mean \pm SD of 2 cells). Sharp wave-ripple events occurred during CA2 3-Hz intracellular oscillation periods as well as nonoscillation period; of 43 events, 35% events occurred during CA2 3-Hz intracellular oscillation periods, and thus, the occurrence frequency was lower during the oscillation periods ($P = 6.72 \times 10^{-2}$, $Z = 1.83$, Z -test for a proportion versus 50%). During the oscillation periods, sharp wave-ripple events (measured as the timings of ripple peaks) occurred at phases of $170^\circ \pm 62^\circ$ of the CA2 3-Hz oscillations and was significantly clustered around the trough (180°) of the 3-Hz oscillations ($P < 0.005$, $V_{15} = 2.98$, V -test versus 180°). We also statistically extracted the 3-Hz component from CA1 LFPs and calculated the phase of CA2 spikes in CA1 LFP 3-Hz cycles. The mean phase was $151^\circ \pm 102^\circ$ and was significantly clustered near the trough of the oscillations ($P < 0.0001$, $V_{352} = 4.83$, V -test versus 180°). These findings validated that in the two neurons, the CA2 V_m dynamics were functionally linked to the CA1 LFPs. Nonetheless, interestingly, the 3-Hz oscillations of the CA2 pyramidal cells *per se* were not associated with the CA1 LFP oscillations. This conclusion was determined using five different methods, (i) wavelet transform analyses (Fig. 5D), (ii) wavelet coherence analyses (Fig. 5E; note that the phases at the coherence peaks were unstable over time), (iii) power correlation analyses (Fig. 5F), (iv) coherence analyses (Fig. 5G; note that the coherence peaks were less than 0.1 in both cells), and (v) fast Fourier transform analyses (Fig. 5H; note that there was no overlapped peak at 3 Hz). Moreover, we examined whether CA2 V_m oscillations were associated with gamma-frequency (30–90 Hz) oscillations in CA1 LFPs. However, we did not find that CA1 gamma oscillations were significantly linked to the CA2 intracellular 3-Hz periods (data not shown). Taken together, these findings suggest that 3-Hz oscillations reflect a local neuronal process in the CA2 region rather than a larger-scale process by the entire hippocampal network.

Finally, we used acutely prepared hippocampal slices. Via bath-perfusion with 1 μ M tetrodotoxin, we blocked action

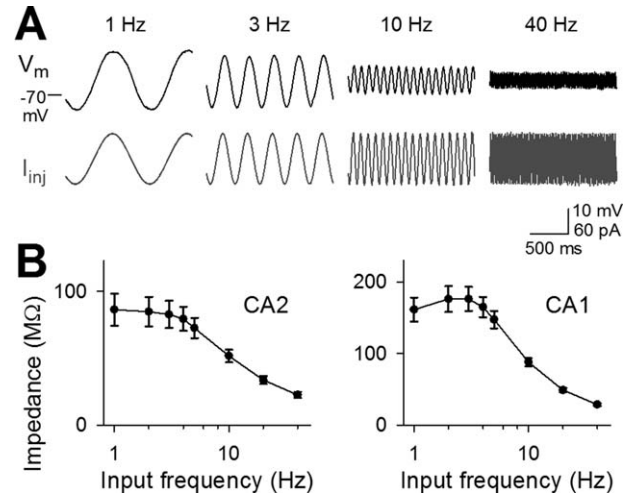


FIGURE 6. CA2 pyramidal cells are not intrinsically resonant with 3-Hz sinusoidal inputs: *in vitro* slice experiments. **A**, Representative V_m traces (*top*) of a CA2 pyramidal cell in response to sinusoidal current injections at frequencies of 1, 3, 10, and 40 Hz (*bottom*) are shown. **B**, The mean membrane impedances of CA2 (*left*) and CA1 (*right*) neurons were plotted as a function of the frequencies of sinusoidal current inputs. Error bars represent the SEMs of 10 CA2 cells (*left*) and 6 CA1 cells (*right*). Experiments were conducted using acute hippocampal slices in the presence of 1 μ M tetrodotoxin.

potentials and recorded V_m of CA2 and CA1 pyramidal cells. We subsequently injected sinusoidal currents at various frequencies into the current-clamped neurons and determined whether their V_m were resonant with specific frequencies of the input stimulus (Fig. 6A). The CA2 neurons did not exhibit a prominent peak impedance at any input frequency (Fig. 6B left), whereas the CA1 pyramidal neurons exhibited a prominent peak at an input frequency of approximately 2–4 Hz (Fig. 6B right; see also Zemankovics et al., 2010). Thus, in contrast to CA1 pyramidal cells, CA2 pyramidal cells are not likely to intrinsically oscillate at an input frequency of 3 Hz.

DISCUSSION

In the present study, we developed a surgical technique that enables whole-cell patch-clamp recordings from CA2 pyramidal cells of the hippocampus in head-restricted mice and monitoring of the ongoing dynamics of V_m from 13 CA2 pyramidal cells. Approximately half of the recorded CA2 pyramidal cells exhibited subthreshold oscillations at ~ 3 Hz, which is an oscillatory pattern that has not been previously described in hippocampal neurons.

The 3-Hz oscillations are in close proximity to the minimum frequency of the theta-oscillation range (Buzsaki, 2002). Therefore, 3-Hz oscillations may be regarded as hippocampal theta oscillations that have been slightly altered as a result of anesthesia (Soltesz and Deschenes, 1993; Ylinen et al., 1995); however, the current findings may disprove this interpretation.

Theta oscillations comprise large-scale events that recruit the entire hippocampal network, including the CA1 and CA3 regions (Lubenov and Siapas, 2009; Mizuseki et al., 2009). Therefore, if the CA2 3-Hz oscillations reflect theta oscillations, they would be synchronized with the CA1 theta oscillations; however, we demonstrated that the CA1 LFPs did not exhibit specific oscillations during the CA2 3-Hz V_m oscillations.

A previous study showed that in urethane-anesthetized rats, CA1 pyramidal neurons exhibit intracellular gamma-frequency oscillations, which may result from the intrinsic resonant properties of these neurons (Penttonen et al., 1998). In contrast, we did not find significant gamma oscillations (30–90 Hz) during either 3-Hz oscillation events or non-oscillation events. Moreover, we failed to find specific resonant properties of the CA2 pyramidal neurons *in vitro*. Thus, the intracellular 3-Hz oscillations of the CA2 neurons are unlikely to result from or impact on the CA1 gamma oscillations.

Because our *in vitro* data indicated that CA2 pyramidal cells do not possess intrinsic membrane properties that resonate at the 3-Hz oscillatory frequency, the intrinsic membrane properties of the CA2 pyramidal neurons cannot fully explain *in vivo* 3-Hz oscillations. On the other hand, CA1 neurons resonated intrinsically with approximately 3-Hz oscillatory inputs (Zemankovics et al., 2010); however, they have not been demonstrated to oscillate at 3-Hz *in vivo*. We demonstrated that 3-Hz oscillations were rare in CA1 pyramidal cells *in vivo*. Thus, whereas CA1 neurons may oscillate at a 3-Hz frequency, this capability is masked under synaptic barrages *in vivo*. In contrast, CA2 neurons did not resonate intrinsically with 3-Hz inputs *in vitro* but did exhibit 3-Hz oscillations. Therefore, we suggest that CA2 3-Hz oscillations are a network phenomenon; they receive specific synaptic inputs that overwhelm the “nonresonant” intrinsic properties. Unfortunately, to date, we have not identified the synaptic inputs or the source regions that produce the CA2 3-Hz oscillations; nevertheless, it is intriguing to demonstrate that CA1 LFPs do not correlate with CA2 3-Hz oscillations. Because the LFPs recorded from the CA1 *stratum radiatum* mainly reflect synaptic inputs from CA3 pyramidal cells and the CA1 local circuits, we speculate that 3-Hz CA2 oscillations are not of CA3 origin. Moreover, several studies have shown that under urethane-induced anesthesia, the 4-Hz extracellular oscillations are observed in the supramammillary nucleus of the hypothalamus (Kocsis and Kaminski, 2006; Kowalczyk et al., 2014), the brain region that projects to the CA2 region, but not to the CA1 or CA3 region (Vertes, 2015). Thus, the 3-Hz intracellular oscillations in the CA2 may be provided by CA2 local circuits or extra-hippocampal afferents from the diencephalon.

The functional role of 3-Hz oscillations remains unclear; however, the current work highlights several important future research directions. First, 4-Hz oscillations have been reported in other brain regions, including the medial prefrontal cortex and the ventral tegmental area (Fujisawa and Buzsaki, 2011). These 4-Hz oscillations are time-locked to the hippocampal theta oscillations and are enhanced during a working memory

task. Similar 4-Hz synchronizations occur between the prefrontal cortex and the amygdala and modulate fear behaviors (Karalis et al., 2016). We did not examine whether CA2 3-Hz oscillations are synchronized with the activity of other brain regions; however, we predict that an analysis of the inter-region correlations with CA2 3-Hz oscillations may indicate the physiological role of 3-Hz oscillations and their neural source. Second, we demonstrated that CA2 3-Hz oscillations intermittently emerged. It remains to be clarified whether 3-Hz oscillations are linked to a specific network or behavioral state. CA2 3-Hz oscillations may reflect a functional aspect of cognitive function. Third, we determined that not all CA2 pyramidal cells oscillate at 3 Hz. Three-hertz oscillating and nonoscillating cells largely shared common electrophysiological properties; however, the two cell types may comprise heterogeneous subpopulations and thus have different roles. Consistent with this speculation, a recent study that used extracellular recording techniques indicated that the CA2 region has a distinct neuronal population that signals the location of an animal during times of immobility (Kay et al., 2016). Whole-cell recordings from CA2 neurons of freely behaving animals may demonstrate the relationship between intracellular oscillations and behavioral function.

REFERENCES

- Abe R, Sakaguchi T, Matsumoto N, Matsuki N, Ikegaya Y. 2014. Sound-induced hyperpolarization of hippocampal neurons. *Neuroreport* 25:1013–1017.
- Amaral D, Lavanex P. 2007. Hippocampal neuroanatomy. In: Andersen PMR, Amaral D, Bliss T, O'Keefe J, editors. *The Hippocampus Book*. Oxford, New York: Oxford University Press. pp 37–114.
- Andersen P, Bliss TV, Skrede KK. 1971. Lamellar organization of hippocampal pathways. *Exp Brain Res* 13:222–238.
- Buzsaki G. 2002. Theta oscillations in the hippocampus. *Neuron* 33:325–340.
- Caruana DA, Alexander GM, Dudek SM. 2012. New insights into the regulation of synaptic plasticity from an unexpected place: Hippocampal area CA2. *Learn Mem* 19:391–400.
- Fujisawa S, Buzsaki G. 2011. A 4 Hz oscillation adaptively synchronizes prefrontal, VTA, and hippocampal activities. *Neuron* 72:153–165.
- Funayama K, Minamisawa G, Matsumoto N, Ban H, Chan AW, Matsuki N, Murphy TH, Ikegaya Y. 2015. Neocortical rebound depolarization enhances visual perception. *PLoS Biol* 13:e1002231.
- Harvey CD, Collman F, Dombeck DA, Tank DW. 2009. Intracellular dynamics of hippocampal place cells during virtual navigation. *Nature* 461:941–946.
- Hitti FL, Siegelbaum SA. 2014. The hippocampal CA2 region is essential for social memory. *Nature* 508:88–92.
- Ishikawa D, Matsumoto N, Sakaguchi T, Matsuki N, Ikegaya Y. 2014. Operant conditioning of synaptic and spiking activity patterns in single hippocampal neurons. *J Neurosci* 34:5044–5053.
- Jones MW, McHugh TJ. 2011. Updating hippocampal representations: CA2 joins the circuit. *Trends Neurosci* 34:526–535.
- Karalis N, Dejean C, Chaudun F, Khoder S, Rozeske RR, Wurtz H, Bagur S, Benchenane K, Sirotta A, Courtin J, Herry C. 2016. 4-Hz

- oscillations synchronize prefrontal-amygdala circuits during fear behavior. *Nat Neurosci* 19:605–612.
- Kay K, Sosa M, Chung JE, Karlsson MP, Larkin MC, Frank LM. 2016. A hippocampal network for spatial coding during immobility and sleep. *Nature* 531:185–190.
- Kocsis B, Kaminski M. 2006. Dynamic changes in the direction of the theta rhythmic drive between supramammillary nucleus and the septohippocampal system. *Hippocampus* 16:531–540.
- Kowalczyk T, Bocian R, Caban B, Konopacki J. 2014. Atropine-sensitive theta rhythm in the posterior hypothalamic area: In vivo and in vitro studies. *Hippocampus* 24:7–20.
- Kuga N, Sasaki T, Takahara Y, Matsuki N, Ikegaya Y. 2011. Large-scale calcium waves traveling through astrocytic networks in vivo. *J Neurosci* 31:2607–2614.
- Lubenov EV, Siapas AG. 2009. Hippocampal theta oscillations are travelling waves. *Nature* 459:534–539.
- Makino K, Funayama K, Ikegaya Y. 2016. Spatial clusters of constitutively active neurons in mouse visual cortex. *Anat Sci Int* 91:188–195.
- Mankin EA, Diehl GW, Sparks FT, Leutgeb S, Leutgeb JK. 2015. Hippocampal CA2 activity patterns change over time to a larger extent than between spatial contexts. *Neuron* 85:190–201.
- Mizunuma M, Norimoto H, Tao K, Egawa T, Hanaoka K, Sakaguchi T, Hioki H, Kaneko T, Yamaguchi S, Nagano T, et al. 2014. Unbalanced excitability underlies offline reactivation of behaviorally activated neurons. *Nat Neurosci* 17:503–505.
- Mizuseki K, Sirota A, Pastalkova E, Buzsaki G. 2009. Theta oscillations provide temporal windows for local circuit computation in the entorhinal-hippocampal loop. *Neuron* 64:267–280.
- Pagani JH, Zhao M, Cui Z, Avram SK, Caruana DA, Dudek SM, Young WS. 2015. Role of the vasopressin 1b receptor in rodent aggressive behavior and synaptic plasticity in hippocampal area CA2. *Mol Psychiatry* 20:490–499.
- Penttonen M, Kamondi A, Acsady L, Buzsaki G. 1998. Gamma frequency oscillation in the hippocampus of the rat: Intracellular analysis in vivo. *Eur J Neurosci* 10:718–728.
- Piskorowski RA, Nasrallah K, Diamantopoulou A, Mukai J, Hassan SI, Siegelbaum SA, Gogos JA, Chevaleyre V. 2016. Age-dependent specific changes in area CA2 of the hippocampus and social memory deficit in a mouse model of the 22q11.2 deletion syndrome. *Neuron* 89:163–176.
- Sakaguchi T, Ishikawa D, Nomura H, Matsuki N, Ikegaya Y. 2012. Normal learning ability of mice with a surgically exposed hippocampus. *Neuroreport* 23:457–461.
- Smith AS, Williams Avram SK, Cymerblit-Sabba A, Song J, Young WS. 2016. Targeted activation of the hippocampal CA2 area strongly enhances social memory. *Mol Psychiatry* 21:1137–1144.
- Soltész I, Deschenes M. 1993. Low- and high-frequency membrane potential oscillations during theta activity in CA1 and CA3 pyramidal neurons of the rat hippocampus under ketamine-xylazine anesthesia. *J Neurophysiol* 70:97–116.
- Valero M, Cid E, Averkin RG, Aguilar J, Sanchez-Aguilera A, Viney TJ, Gomez-Dominguez D, Bellistri E, de la Prida LM. 2015. Determinants of different deep and superficial CA1 pyramidal cell dynamics during sharp-wave ripples. *Nat Neurosci* 18:1281–1290.
- Vertes RP. 2015. Major diencephalic inputs to the hippocampus: Supramammillary nucleus and nucleus reuniens. *Circuitry and function. Prog Brain Res* 219:121–144.
- Ylinen A, Soltész I, Bragin A, Penttonen M, Sik A, Buzsaki G. 1995. Intracellular correlates of hippocampal theta rhythm in identified pyramidal cells, granule cells, and basket cells. *Hippocampus* 5:78–90.
- Zemankovics R, Kali S, Paulsen O, Freund TF, Hajos N. 2010. Differences in subthreshold resonance of hippocampal pyramidal cells and interneurons: The role of h-current and passive membrane characteristics. *J Physiol* 588:2109–2132.